Journal of Nuclear Materials 392 (2009) 510–518

Contents lists available at ScienceDirect

Journal of Nuclear Materials

journal homepage: www.elsevier.com/locate/jnucmat

Physical properties of an alumino-silicate waste form for cesium and strontium

M.D. Kaminski *, C.J. Mertz, M. Ferrandon, N.L. Dietz, G. Sandi

Chemical Sciences and Engineering Division, Argonne National Laboratory, 9700 South Cass Avenue, Argonne, IL 60439, United States

ARTICLE INFO

Article history:
Received 20 January 2009
Accepted 21 April 2009

PACS:
81.05.Je

ABSTRACT

Nuclear fuel reprocessing will be required to sustain nuclear power as a baseload energy supplier for the world. New reprocessing schemes offer an opportunity to develop a better strategy for recycling elements in the fuel and preparing stable waste forms. Advanced strategies could create a waste stream of cesium, strontium, rubidium, and barium. Some physical properties of a waste form containing these elements sintered into bentonite clay were evaluated. We prepared samples loaded to 27% by mass to a density of approximately 3 g/cm^3. Sintering temperatures of up to 1000 °C did not result in volatility of cesium. Instead, the crystallinity noticeably increased in the waste form as temperatures increased from 600 to 1000 °C. Assemblages of silicates were formed. Significant water evolved at approximately 600 °C but no other gases were generated at higher temperatures.

1. Introduction

To date, spent nuclear fuel reprocessing has been limited to recovery of plutonium and uranium. Therefore, the liquid waste generated during reprocessing is described by a very complex chemistry. To stabilize such a mixture for disposal requires a waste form with adequate flexibility. The waste form chosen in the US and abroad is borosilicate glass. If, however, advanced separations are conducted on the waste, purified waste streams may be produced that would simplify the chemistry of the waste. As a result, one can envision using waste forms other than glass that may prove simpler to fabricate and reduce costs, while maintaining regulatory compliance. For example, future reprocessing activities, as being designed under the Advanced Fuel Cycle Initiative and schemes for treating the legacy nuclear weapons liquid waste stored in underground tanks at several DOE sites may eliminate key radionuclides from the glass waste form. Two elements of interest are cesium and strontium because ^{137}Cs and ^{90}Sr isotopes will be responsible for a significant heat-load during disposal. If these are isolated, then the overall waste form volume for cesium and strontium may be reduced.

Within advanced reprocessing schemes, cesium and strontium would be isolated along with rubidium and barium due to their chemical similarity during solvent extraction. In one study [1], potential candidate waste forms for the cesium and strontium waste stream (containing barium and rubidium) were evaluated. In [2], we described the thermal properties of potential storage media for cesium and strontium separated from nuclear fuel using the UREX+ process. In [3], we described the estimated storage form volumes and potential storage scenarios. However, those studies were performed based on theoretical properties since the fabrication of waste forms containing *both* cesium and strontium is largely novel.

Since the paper by Hatch [4], natural clays have been studied as potential host materials for radioactive waste and especially cesium. Moreover, there is an abundance of information on the formation of pollucite from cesium solutions and alumino-silicates. For example, to produce pollucite, Strachan and Shulz [5] described the formation of pollucite directly from sintering a cesium chloride solution in bentonite clay. They found that sintering at 750 °C for 2 h was required to convert CsCl mixed with bentonite clay into pollucite and the use of caustic cesium chloride and pre-calcining the bentonite lowered the temperature for complete reaction to <650 °C. The maximum loading of cesium to form pollucite was 42.6%. One study [6] described a multi-step process with cesium hydroxide, water, aluminum, powder, and SiO_2 as starting materials to prepare a sol which was hydrothermally processed at 220 °C for 2–24 h to produce a dry powder. They achieved 95% theoretical density after sintering at 1500 °C for 10 h. Yanagisawa et al. [7] created pollucite structures for cesium by hydrothermal alteration of alumino-silicate, quartz, and $Al(OH)_3$. They found that pollucite could be formed at 200 °C under alkaline conditions. Their results also suggest that the anion to cesium might play a significant role in the leaching characteristics of cesium pollucite.

Concerning the alkaline earth metals, Chernyshova et al. [8] prepared strontium and barium feldspars from stoichiometric quantities of the carbonate salts and Al_2O_3 and SiO_2 at 1300–1400 °C. Mimura et al. [9] mobilized cesium into mordenite and strontium into zeolite-A to form pollucite and Sr-feldspars after heating to 1200 °C. Sorrell [10] observed that Ba-feldspars formed

* Corresponding author. Tel.: +1 630 252 4777; fax: +1 630 972 4499.
E-mail address: kaminski@anl.gov (M.D. Kaminski).

0022-3115/$ - see front matter © 2009 Elsevier B.V. All rights reserved.
doi:10.1016/j.jnucmat.2009.04.020

at approximately 1250 °C after heating the sulfate salt in kaolinite while strontium feldspars formed at 1150 °C.

More recently, Tripp et al. [11] converted clay, additives, cesium, and strontium feeds into solidified products by steam reforming but this study focused on the performance of the steam reforming operation and provided only cursory characterization of the solidified product. Vasil'eva et al. [12] describe the formation of cesium pollucite and strontium feldspars or strontium silicates when cesium or strontium was sintered into alumino-silicates derived from fractionated, coal fly ash. However, their study did not combine cesium and strontium into a single feed stream.

Because of simple unit operations, the prospect of forming stable alkali and alkaline-earth alumino-silicate phases, and the desire to test processes that held promise for rapid deployment, we chose to investigate the method described by Strachan and Shulz [5] for stabilizing cesium and strontium. Here, we describe the physical properties of alumino-silicate ceramic waste forms fabricated from bentonite clay, composed predominantly of montmorillonite. We sintered bentonite clay containing cesium, strontium, rubidium, and barium salts in air. We investigated the physical properties of various sintered samples, some basic thermal properties, and analyzed the gas evolved during sintering. The release of water peaked in its evolution at approximately 600 °C. This was accompanied by NO_x species. The crystallinity of the waste form increased with increasing temperature up to 1000 °C as evidenced by X-ray diffraction. The final waste product was hard and brittle with a true density of 3 g/cm^3, 44% porosity, and measured loading of 26.9% by mass of cesium, strontium, rubidium, and barium. The thermal conductivity of the porous material was 1.50–1.95 W/m/K.

2. Methods

Deionized water was obtained from in-house supply. The strontium nitrate and chloride salts were reagent grade. The bentonite clay was a sodium bentonite (Volclay HPM-20, 425 mesh, American Colloid Company, Belle Fourche, SD) that was air purified and classified at the plant. It contained 12% moisture and was used as received. The vendor supplied a technical data sheet of the elemental composition of the material that was corroborated by X-ray fluorescence conducted at the University of Nevada Las Vegas (personal communication with Dr G. Cerefice, Harry Reid Center, UNLV). The moisture free composition reported by American Colloid was SiO_2 = 69.56%, Al_2O_3 = 20.69%, MgO = 2.70%, Fe_2O_3 = 4.85%, CaO = 1.30%, Na_2O = 2.43%, K_2O = 0.30%. The loss-on-ignition was 4.80%. The specific gravity was 2.6 and the pH of a 2% solid suspension was 8.5–10.5.

2.1. Cesium and strontium waste feed compositions

The potential waste solutions containing cesium, strontium, barium, and rubidium varies depending on the specifics of a reprocessing scheme. We prepared three different types of stock solutions to capture a range of potential feeds.

A 'chloride feed solution' was prepared with Cs, Sr, Rb, and Ba concentrations of 0.565 M Cs^+, 0.427 M Sr^{2+}, 0.141 M Rb^+, and 0.719 M Ba^{2+} as the chloride salts. Such a waste stream could be generated after electrochemical reprocessing of spent fuel.

A 'nitrate feed solution' was prepared using nitrate salts at one fifth the chloride waste stream concentrations of the alkali and alkaline earth elements reported in the above paragraph due to the limited solubility of the nitrate salts of cesium and barium at the waste stream concentrations. Such a waste stream could be generated after solvent extraction reprocessing of spent fuel using the FPEX process [13] or from acidification of nuclear tank waste.

An additional feed stock solution was prepared based upon a strip solution from the CCD-PEG process [14] ('CCD-PEG simulated strip solution'). This sample was prepared to compare off-gas species with the 'nitrate-feed stock solution'. The CCD-PEG stock solution was prepared with the following composition: 0.293 g/L $CsNO_3$, 0.242 g/L $Sr(NO_3)_2$, 0.0555 g/L $RbNO_3$ and 0.500 g/L $Ba(NO_3)_2$, 100 g/L guanidine carbonate and 20 g/L diethylenetriaminepentaacetic acid (DTPA).

2.2. Sample preparation for bentonite clay loaded with the chloride and nitrate salt feed solution

The chloride feed solution (27.9 mL, 0.565 M Cs^+, 0.427 M Sr^{2+}, 0.141 M Rb^+, and 0.719 M Ba^{2+}) was added to 15 g of as-received clay, mixed, and dried overnight at 60 °C. In addition, this feed solution was diluted by 2 and 4 and added in the same proportion to produce samples at progressively lower loadings. The total theoretical loading of Cs, Sr, Rb, and Ba were 29%, 16%, and 8% by mass. The theoretical elemental loadings were 9.9%, 4.9%, 1.6%, and 13.0% for Cs, Sr, Rb, and Ba, respectively, for 29% loading. Loading at 16% and 8% followed the same elemental proportions.

The nitrate feed solution (27.9 mL, at 1/5 the cation concentrations of the chloride feed) was added to 15 g of clay. The mixture was homogenized, dried overnight at 60 °C, and then another 27.9 mL was added, homogenized, and dried. These steps were repeated for a total of five times (139.5 mL) to achieve a theoretical elemental loading identical to the chloride feed samples (29% at the same relative elemental proportions). The dried waste-loaded clay samples were mixed by mortar and pestle and samples were prepared for analyses accordingly.

A sample containing the CCD-PEG simulated strip solution was prepared by adding 10 mL of CCD-PEG simulated strip solution to 5-g of bentonite clay. This mixture was homogenized with a glass stir rod and dried at 50 °C overnight. The dried clay sample was mixed by mortar and pestle and a portion of the sample was submitted for off-gas and thermal gravimetric (TGA) analyses.

2.3. Sample pressing and sintering

Small monoliths were prepared after drying the waste-loaded clay samples. The powder was added to a cylindrical die (either 0.5 in., 0.634 in., 0.75 in., or 1–1/8 in. diameter dies) and pressed to 5000, 7900, 10 000, or 15,000 psi. Then, samples were heated from room temperature at 5 °C/min in a Lindberg Blue Furnace or Fisher Scientific Isotemp® Programmable Furnace calibrated against pyrometric cones (Orton Ceramics, Westerville, Ohio). Samples were kept at peak temperature (600–1000 °C) for 12 h and slowly cooled (5 °C/min) to room temperature.

2.4. Bulk density

The bulk density of monolith samples was calculated by measuring the geometric dimensions of the cylindrical sample using digital calipers (Mitutoyo Digimatic Caliper) and weighing the sample (Mettler balances).

2.5. Porosity

The open porosity density (true density) of sintered samples was measured using a Micropycnometer (Quantachrome, MPY-5) run with pure helium gas. A monolithic or crushed sample was placed in the sample cell and weighed. Two grab samples were analyzed and the average value and range was reported. The instrument was calibrated against standard stainless steel spheres. To check the accuracy of this unit against monolithic samples and confirm that the true density was being measured, some samples

were crushed and their density compared to their monolithic measurements. They were in agreement in all cases. The porosity was calculated from the ratio of the bulk and true density.

2.6. Electron microscopy

Clay samples were mounted in epoxy and polished down to a 1 μm diamond paste. Samples were analyzed without further treatment. The Jeol JSM-6400 or Hitachi S-4700 scanning electron microscope, at an accelerating voltage of 3–20 kV, was coupled to an energy dispersive X-ray analyzer.

2.7. Elemental analysis

Neutron activation analysis was performed on five bentonite clay samples. Samples were ground to a powder by mortar and pestle, sealed in polyethylene capsules, and irradiated in a TRIGA reactor (University of Texas, Austin, TX). Four of the samples included cesium, barium, rubidium, and strontium nitrate salts loaded into the clay and were processed as follows: (1) unsintered, (2) sintered at 600 °C, (3) sintered at 800 °C, and (4) sintered at 1000 °C. The fifth sample was a control consisting of the bentonite clay. Barium and strontium were analyzed on triplicate samples in the tPNT mode at 165.8 keV for Ba-139 and at 388 keV for Sr-87 m. Cesium and rubidium were analyzed on duplicate samples in the RSR mode at 604.7 and 795.8 keV for Cs-134 and at 1077 keV for Rb-86. Expressed values are reported as the average and standard error.

2.8. Thermal properties

Thermal properties testing was performed from 23–1000 °C (Thermophysical Properties Research Laboratory, West Lafayette, Indiana). Thermal diffusivity (α) was measured using laser flash technique. Specific heat (C_p) was measured using a differential scanning calorimeter. The thermal conductivity was calculated from $k = \alpha C_p$. Specific heat was measured with sapphire as the standard reference material.

2.9. X-ray diffraction

Samples were analyzed by X-ray diffraction using a Rigaku D/max Rotating Anode Diffractometer equipped with a vertical goniometer using copper Kα radiation. The software program used to analyze the diffraction pattern was Jade 5.0 (Materials Data Inc.) and it used standard search/match parameters to compare the unknown diffraction pattern against powder diffraction patterns supplied by the International Centre for Diffraction Data. Diffractions patterns were obtained under the following conditions: operating parameters: 40 kV, 175 mA; scan speed: 2.4°/min; scan angle: 10–80°.

2.10. Thermal gravimetric analysis

A 10 mg sample was taken in a 70 μl alumina pan and heated from 25 to 800 °C in a thermogravimetric analyzer (Mettler Toledo TGA/SDTA 851E) at a rate of 5 °C/min in O_2 with a flow rate of 60–90 mL/min.

2.11. Off-gas analysis

The temperature-programmed gas evolution studies were conducted by measuring the product yield as a function of temperature using a commercial characterization system (Zeton Altamira, Model AMI-100). A powder sample of 100 mg was heated from room temperature to 1000 °C at a rate of 2 °C/min in a gas mixture of 4% O_2 in He at a flow rate of 50 mL/min. The temperature was monitored using an Omega Type K thermocouple located at the exit of the sample bed. The product gas concentration was analyzed for CO, CO_2, H_2O, NH_3, NO, NO_2, N_2O, HCN, Cs, and CsOH using a Dycor Dymaxion quadrupole mass spectrometer.

3. Results

The bentonite clay was off-white in color and, when sintered at 1000 °C, formed a friable rust-orange mass (Fig. 1). When loaded with the radionuclides (29 mass% of Cs, Sr, Rb, Ba), it sintered at 800–1000 °C to a hard, yellow-white mass (Fig. 1).

From electron microscopy, it was clear that at 800 °C, the sintering of particle grains was incomplete as the morphology was dominated by small, individual grains. At 1000 °C, the particle grains were fused revealing a much more continuous network riddled with clusters of pores (pictures not shown). Elemental mapping showed a uniform distribution of cesium, strontium, and barium (Rb could not be detected by EDS reliably) with no noticeable concentration of these elements within any phases (Fig. 2).

The radial compaction of the samples was 2–4% at 1000 °C but the radius increased by 2% when sintered at 800 °C. When we decreased the loading of surrogate radionuclides into the bentonite, the compaction increased slightly, being 6% at 8.4 wt% loading. The density of the sintered clay was affected by the loading of surrogate radionuclides (Fig. 3); an increase in loading from 8% to 29% increased the porosity of the final form from 21% to 47%.

The pressure that was used to form the green (unsintered) compact had little effect on the true density for samples that sintered at 600–1000 °C. However, the porosity showed a slight decrease with an increase in the compacting pressure for pressures greater than 5000 psi. We measured a porosity of 44% at 5000 psi compared to 36% at 15 000 psi.

3.1. Thermal properties

We measured the thermal properties of the sintered (1000 °C for 12 h) bentonite clay loaded to 29%. The specific heat of the material increased by 42% as the temperature increased from room temperature to 1000 °C (Fig. 4). The thermal diffusivity of the sintered bentonite material was not sensitive to temperature over the same range (Fig. 4). The thermal conductivity (Fig. 5) increased from 1.50 W/m/K to 1.95 W/m/K as the temperature increased from room temperature to 1000 °C.

3.2. Elemental and mineral composition

The diffraction pattern for the bentonite clay starting material identified montmorillonite as the major phase. In addition, quartz

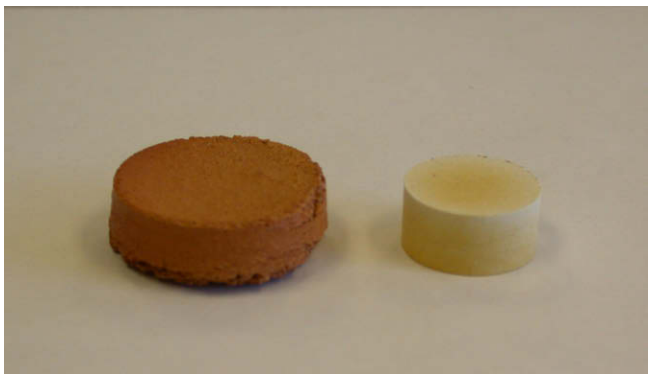

Fig. 1. Sintered bentonite clay (left) and sintered bentonite containing the Cs, Sr, Rb, and Ba chloride feed solution (right, 29% waste loading). Sample was sintered at 1000 °C for 12 h.

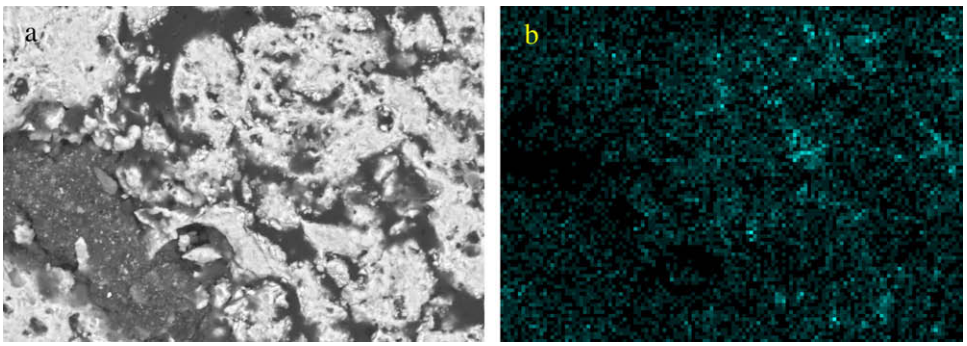

Fig. 2. (a) Backscatter electron micrograph of sintered bentonite containing Cs, Sr, Rb, Ba loaded to 29% from the chloride feed solution. White areas are the crystalline phases and the dark areas designate pores filled by the epoxy mounting media. (b) X-ray mapping of same showing cesium (lighter pixels) distributed throughout the matrix. Strontium and barium showed a similar distribution.

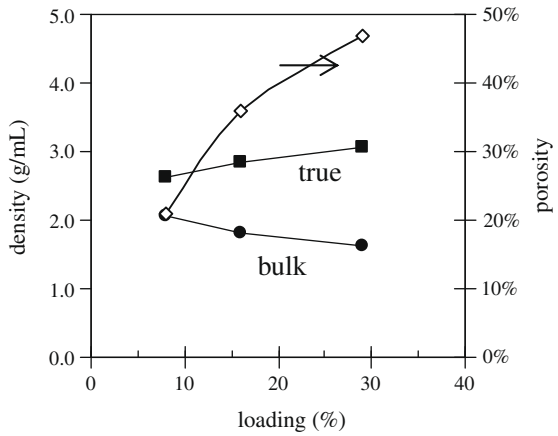

Fig. 3. Effect of different waste loadings on the bulk density (circles, solid), true density (squares, solid), and porosity (diamonds, open) of bentonite monoliths containing radionuclide surrogates (chloride feed solution) sintered at 1000 °C for 12 h.

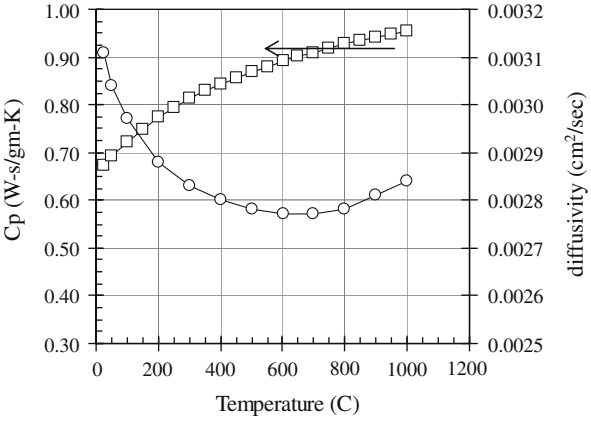

Fig. 4. Specific heat (squares) and thermal diffusivity (circles) of sintered bentonite containing 29 mass% of Cs, Sr, Rb, Ba from the chloride feed solution (sintered at 1000 °C for 12 h).

and potassium alumino-silicate phases were identified. A relatively large amorphous or nanocrystalline component was present in the clay, indicated by peak broadening.

We used X-ray diffraction to monitor the mineral composition and crystallinity of the materials as a function of sintering temperature (Fig. 6). The X-ray data showed a distinct transformation

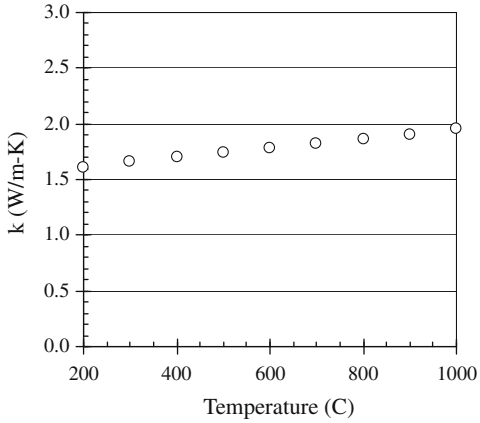

Fig. 5. Thermal conductivity of sintered bentonite containing 29 mass% of Cs, Sr, Rb, Ba from the chloride feed solution (sintered at 1000 °C for 12 h).

above 700 °C, noted by a decrease in the amorphous scattering background at low 2θ.

Interestingly, the X-ray diffraction pattern differed slightly between samples prepared with the chloride feed solution and nitrate feed solution (Fig. 7). For the samples prepared with the chloride feed stock solution, the peaks correlate well with barium alumino-silicates ($Ba_{0.5}Sr_{0.5}Al_2Si_2O_8$ and $Ba_{0.75}Sr_{0.25}Al_2Si_2O_8$) including celsian ($BaAl_2Si_2O_8$). Interestingly, no pollucite was confirmed. In fact, we could not positively identify cesium phases. To investigate this further, we prepared samples with progressively lower concentrations of surrogate radionuclides to see if pollucite would form at lower waste loadings. There was an absence of the pollucite signature peaks even at 8% loading of the clay.

In contrast, the samples prepared with the nitrate feed solution were dominated by pollucite phases ($CsAlSi_2O_6$) and iron pollucite ($Cs_2Fe_2Al_2Si_4O_{12}$), Ba-orthoclases [$(K,Ba)(Si,Al)_4O_8$], and possibly a rubidium–iron–silicate ($Rb_2FeSi_5O_{12}$) (Fig. 7).

3.3. Off-gas analysis

We compared the composition of the gas evolved during sintering of samples dried to 60 °C overnight (Table 1). Cesium was not detected in the off-gas analyses (as Cs^0 and CsOH) for the waste-loaded clay samples for temperatures up to 900 °C in 4% O_2/He. A major off-gas species for all the clay samples was water (Fig. 8). All of the clay samples showed water losses at less than 100 °C indicating weakly-bound surface water. Additional water loss peaked at 680 °C for the clay and 600 °C for the waste-loaded clay

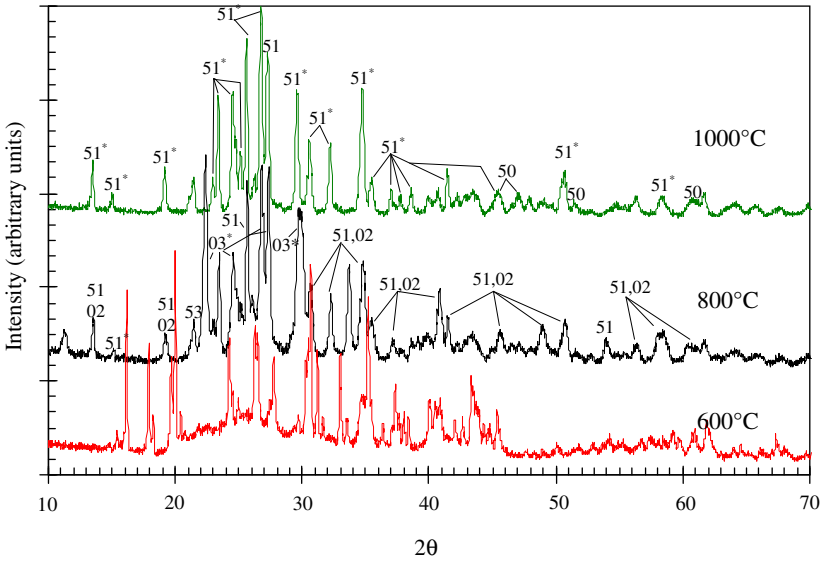

Fig. 6. X-ray diffraction pattern of sintered bentonite prepared with the chloride feed solution and containing 29 mass% of Cs, Sr, Rb, Ba at 1000 °C (top), 800 °C (middle) and 600 °C (bottom). The 700 °C data (not included) was not significantly different than the 600 °C pattern. Note: the amorphous background at $2\theta = 20–30°$ was suppressed at higher sintering temperatures. At 600 °C, all peaks $<2\theta = 50°$ are assigned to $BaCl_2$ hydrate ICDD 25-1135. '51' refers to $Ba_{0.75}Sr_{0.25}Al_2Si_2O_8$ ICDD 38-1451; '51*' refers to ICDD-38-1451 and 38-1453, $Ba_{0.25}Sr_{0.75}Al_2Si_2O_8$; '50' refers to celsian, ICDD 38-1450; '02' refers to orthoclase ICDD 19-0002; '03' refers to orthoclase ICDD 19-0003, '03*' can be assigned to the orthoclases and barium strontium alumino-silicates.

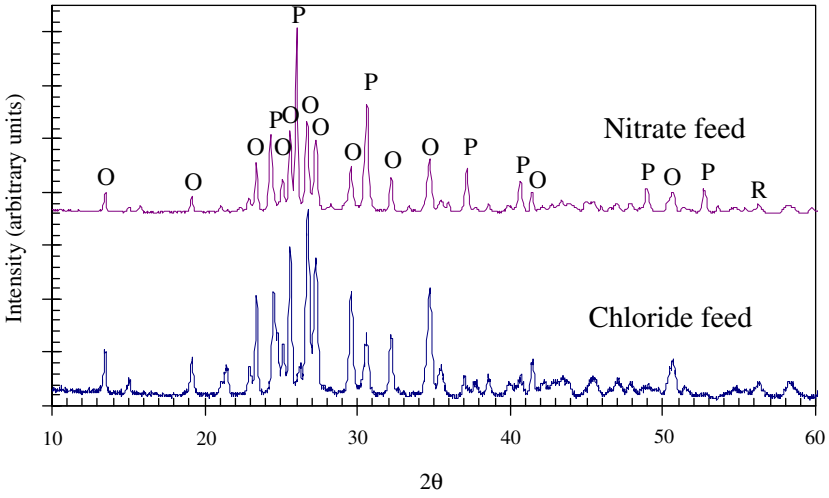

Fig. 7. X-ray diffraction patterns of bentonite clay loaded with chloride feed solution or nitrate feed solution (P = pollucite, O = orthoclase, R = rubidium iron silicate, minor peaks at $2\theta > 60°$ correlate with iron pollucite phases). The peaks from the chloride feed sample all correlated well with barium alumino-silicates (see Fig. 6). Samples were loaded to 29% and sintered at 1000 °C for 12 h.

Table 1
Temperatures (°C) of peak maxima for off-gas species in bentonite and loaded with CCD-PEG simulated strip or nitrate feed solution.

Off-gas species	Clay only	Clay loaded with CCD-PEG simulated strip	Clay loaded with nitrate feed
Cs	ND	ND	ND
CsOH	N/A	N/A	ND
H_2O	⩽100, 675 (#)	⩽100, 200, 280, 610 (#)	⩽100, 590 (#)
N_2O, CO_2	630	200, 300, 460, 600 (#)	370, 550, >900
NO	ND	200, 300, 600	590 (#)
NO_2	ND	ND	580
CO, N_2	ND	200, 470, 600	350, 650

ND = none detected.
N/A = not analyzed.
(#) = major species.

samples corresponding to dehydroxylation of the clay. Accompanying the water loss at 600 °C were other species. Nitric oxide (Figs. 9 and 10) was a major off-gas component at 600 °C from waste-loaded samples. CO_2 was driven from the CCD-PEG waste

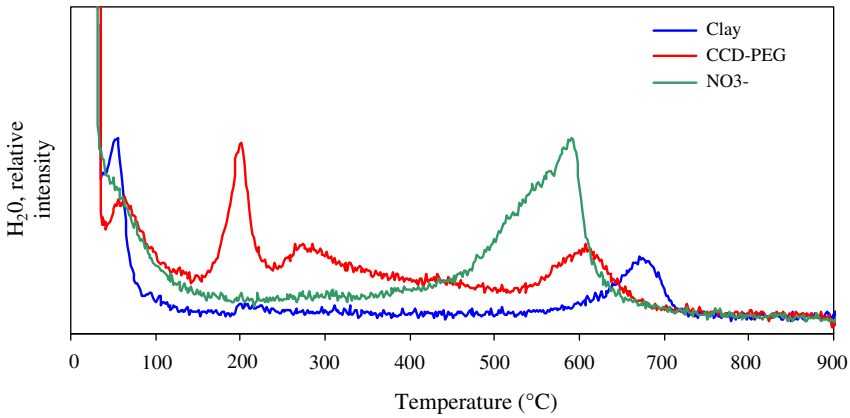

Fig. 8. Off-gas analysis of water from bentonite clay (blue) and bentonite clay loaded with the CCD-PEG simulated strip solution (red) or nitrate feed solution (green).

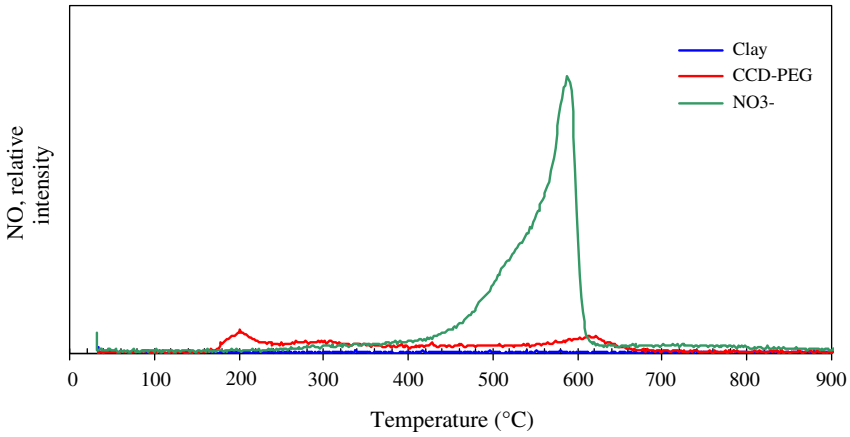

Fig. 9. Off-gas analysis of NO from bentonite clay (blue) and bentonite clay loaded with the CCD-PEG simulated strip solution (red) or nitrate feed solution (green).

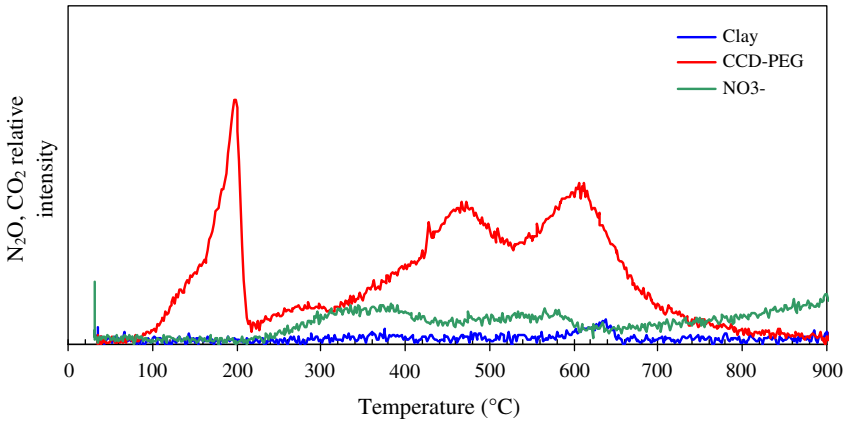

Fig. 10. Off-gas analysis of N_2O and/or CO_2 species from bentonite clay (blue) and bentonite clay loaded with the CCD-PEG simulated strip solution (red) or nitrate feed solution (green).

with peaks at 200, 280, and 610 °C. These peaks correspond to the peaks identified as interlayer water (Fig. 8) suggesting a contribution from the decomposition of organic species into CO_2 and H_2O. Other nitrogen and carbon species were detected at much lower levels and were lost at temperatures corresponding to the major off-gas species (Table 1).

There was no significant change in the relative concentrations of Cs, Rb, Sr, Ba as a function of sintering temperature from 600 to 1000 °C, indicating that volatile species (water, gases) were driven off by 600 °C. All waste component concentrations in the sintered samples increased by 25% when compared with the unsintered, waste-loaded clay sample (Table 2). This increase can be accounted for in the water and NO_x losses that occurred during sintering of the clay samples. The final measured loading was 26.9% by mass after sintering to 1000 °C (8.8% Cs, 4.6% Sr, 1.6% Rb, 11.9% Ba) from a target of 29.4%.

Table 2
Concentration of some elements in the bentonite clay samples loaded with the nitrate salt feed containing Cs, Sr, Rb, and Ba (theoretical loading = 29.4%).

Element	Clay	Loaded dry	600 °C	800 °C	1000 °C
Al	107 600 ± 1200	64 210 ± 760	78 610 ± 980	80 580 ± 900	81 260 ± 940
Ca	9950 ± 620	6000 ± 380	7660 ± 430	7180 ± 440	7590 ± 440
Mn	65 ± 3	43 ± 2	52 ± 2	57 ± 2	53 ± 2
Na	13 950 ± 170	8350 ± 91	9980 ± 110	10 460 ± 130	10 340 ± 110
Ti	780 ± 119	484 ± 117	750 ± 126	660 ± 136	585 ± 110
Fe	24 030 ± 930	13 030 ± 2210	14 110 ± 2740	16 750 ± 2750	13 410 ± 2720
Cs	22 ± 1	70 450 ± 240	88 740 ± 300	89 410 ± 300	87 860 ± 300
Sr	369 ± 150	37 260 ± 345	44 090 ± 410	46 090 ± 440	45 690 ± 420
Rb	BDL	13 020 ± 200	16 230 ± 250	16 410 ± 250	16 330 ± 250
Ba	BDL	99 130 ± 620	116 100 ± 720	122 440 ± 770	119 380 ± 740

Note: Conc (concentration) and error are average values.

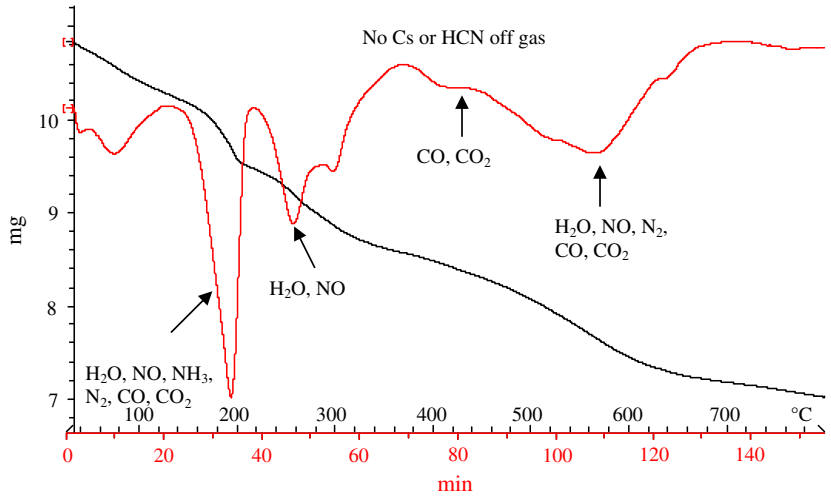

Fig. 11. Weight loss and first-derivative curves from thermal gravimetric analysis of the CCD-PEG simulated strip solution loaded into bentonite clay (in O_2).

3.4. Thermal gravimetry

Three major transitions were observed during the sintering of the CCD-PEG loaded waste sample (Fig. 11): (1) 6.2% loss at $\leqslant$100 °C due to absorbed and weakly bound water, (2) 15% loss from 150–400 °C corresponding to CO_2 or N_2O species and interlayer water (CO_2 and N_2O are indistinguishable in our system since they appear at mass number 44), and (3) 14% loss of CO_2 or N_2O species and water due to dehydroxylation of the clay with a maximum peak ~600 °C. Samples containing the chloride and nitrate feed solutions would be expected to release much less NO_x species and be dominated by water off-gas compared to the sample formed from the CCD-PEG simulated strip solution.

4. Discussion

If nuclear power grows as a baseline energy source, the increased high-level waste generated will present a formidable obstacle to public acceptance. Therefore, it is incumbent on the scientific community to reconsider how we design the fuel cycle. Siting a HLW repository meets numerous delays and criticisms. The possibility of siting a second repository is discouraging.

One way to improve public acceptance is to reduce the amount of waste destined for geologic repository. Indeed, advanced reprocessing schemes address many issues related to fuel recycling and waste minimization [15]. Key aspects of advanced schemes is the separation of selective radionuclides so that they may be managed it ways that avoid its disposal in a repository setting. Wigeland et al. [16] describes the impact of separating the short half-lived, high heat-generating elements of cesium and strontium; eliminating them from the HLW packages dramatically increases the storage capacity of the repository due to a significant decrease in the short-term heat load in the repository. If we decide to follow this waste management path, then we need to identify a suitable host matrix for the waste stream containing cesium and strontium.

The properties that are important to co-disposal of cesium and strontium are minimal unit operations required to convert the liquid waste stream to a stabilized waste product, sufficient loading capacity to minimize the number of packages, durability against thermal stresses developed by radioactive decay heat, and durability against the effects of radioactive decay product in-growth ($^{137}Cs^{1+}$ decays to $^{137}Ba^{2+}$, $^{90}Sr^{2+}$ decays to $^{90}Zr^{4+}$).

To date, many studies describe waste forms for cesium or strontium waste streams but information on waste forms combining these two elements is lacking. The requirements for such a waste form may differ dramatically from those pursued in the past for tank wastes, such as within the Department of Energy inventory, which tend to contain low concentrations of radionuclides and are dominated by high concentration of non-radioactive elements such as sodium.

A clay appears to have good potential for stabilizing both cesium and strontium since they form stable minerals with alumino-silicates. Moreover, the clay matrix tolerates high temperatures well. As a first step toward evaluating the suitability of a clay material for stabilizing highly radioactive cesium and strontium we conducted a study of its basic physical properties.

Stabilizing cesium and strontium feeds such as those produced from solvent extraction processes employing CCD-PEG or FPEX is

not confounded by the presence of copious additional elements. Therefore, sintering into clay may require fewer unit operations. The liquid feed can be mixed directly with the clay, heated to drive off water, acid, pressed into pucks, sintered, and packaged. The high temperature of the sintering process will destroy organics and nitrates, as evidenced by the off-gas analyses (Figs. 8–11). The primary gases produced during heating were H_2O (up to 700 °C for pure clay and lower for loaded clays), NO_2, CO_2, N_2O, NO. The production of nitrogen species continued to approximately 600 °C. Sayi et al. [17] reported that below 700 K (427 °C) N_2O is the dominant species over NO and NO_2 but above this NO dominates over the others. Our study did not follow NO_2 species but the dominance of N_2O below 700 K and NO above 700 K is consistent with our results.

The absence of cesium species in the off-gas is consistent with observations by MacLaren et al. [6] who reported no evidence of mass loss in preparing pollucite until sintering temperatures exceeded 1500 °C. Indeed, the work by Hoinkas and Matiske [18] show that the dominant species during cesium volatilization is Cs^+, CsO^+, $Cs_2(NO)^+$, and Cs_2O. Our study interrogated for Cs and CsOH only and found no evidence of their evolution during heating. An additional check against gross loss of cesium is by comparing the ratio of cesium and other known refractory materials. Using aluminum as the refractory element, the Cs/Al, Sr/Al, Ba/Al, and Rb/Al ratios during heating (Table 3) did not change. From this we can infer that less than 2–3% of these species were evolved during heating. Radioactive tracer or collection of off-gas would be required to improve the detection limits for cesium off-gas.

The final water content of the waste form is an important factor since these waste forms could potentially pressurize due to radiolysis of water under the intense beta-particle flux during the disposal period. Because of intense α-decay activity, $^{238}PuO_2$ packages are limited to a residual water content <0.5% by mass. The off-gas data in our samples show that all water is evolved by approximately 700 °C providing strong indication that radiolysis of water will not present an over-pressurization problem during storage. Importantly, heat-of-wetting values measured on montmorillonite suggest that samples sintered to >800 °C are not susceptible to rehydration [19].

When we sintered the surrogate waste streams into the bentonite, we could identify several major phases, but we would expect the samples to be partially vitrified at 1000 °C given the residual silica content of the clay. This begs the question of whether a percentage of the waste elements migrated into a glassy phase, as observed in previous investigations on glassy ceramics and nuclear waste [20]. From microscopy and X-ray analyses (Fig. 2), we could not identify regions concentrated in cesium, strontium, or barium. However, the resolution of the SEM does not preclude the existence of nanocrystalline phases concentrated in cesium or strontium. Indeed, recent TEM analyses [21] suggest that cesium at least partly crystallizes as nanocrystalline phases.

Interestingly, we observed a difference in the mineral assemblage between the feed containing chloride salts and nitrate salts. The chloride salts produced an X-ray pattern that correlated well with barium–strontium alumino-silicates and celsian. Cesium and rubidium phases could not be identified to a good figure of merit (>14). For samples prepared with the nitrate feed solutions, X-ray diffraction showed that cesium was stabilized in pollucite structures ($Cs_2Fe_2Si_4O_{12}$, $CsAlSi_2O_6{\cdot}xH_2O$) and barium in orthoclases ($(K,Ba)(Si,Al)_4O_8$). Rubidium may be found in an iron silicate but the data is inconclusive. Strontium phases could not be positively identified.

The presence of Fe^{3+} within the pollucite structure suggests a possible mechanism for charge compensation that will be required to stabilize the crystal structure against the effects of Ba^{2+} daughter in-growth. However, thermodynamic data to support this claim is lacking.

The identification of barium and cesium in stable mineral phases is an important find. For cesium, it suggests the possibility that the pollucite structure will retain long-lived ^{135}Cs ($T_{\frac{1}{2}} = 2.3 \times 10^6$ y) over the long-term. We draw no conclusions on the retention of ^{137}Cs once it decays to ^{137}Ba, because of the change in oxidation state and size and associated effects on the crystal structure. Studies to address the effects of decay on the crystal structure of pollucite did not find evidence of changes in the pollucite crystal structure [22] but the study admittedly lacked the sensitivity to draw conclusions. Barium stabilization is equally important for this type of waste form because barium is regulated by the Resource Conservation Recovery Act (RCRA). Wastes containing barium must pass the Toxicity Characteristic Leaching Procedure (TCLP) prior to disposal to avoid categorization as mixed-waste. Indeed, a waste form containing radioactive cesium and barium experiences an in-growth of barium due to the decay chain of radioactive cesium. It then becomes a question of regulatory language on whether the waste must meet the TCLP criteria at the time of disposal or if it must continue to pass the TCLP test during the disposal period. Although, the results are preliminary, TCLP tests on the 29% loaded clay sintered to 1000 °C released barium to approximately the regulatory limit of 120 μg/g. If sintered to higher temperatures (1200 °C) the release of barium and strontium was significantly depressed (<15 μg/g) supporting, perhaps, that stable barium and strontium feldspars form at temperatures higher than 1000 °C, as reported by Sorrell [10]. Cesium was released to approximately 5 μg/g. However, these results must be replicated and supplemented by static and dynamic leaching experiments before drawings conclusions.

The final bulk density of the sintered product was 1.6 g/cm^3 at 29% loading, increasing slightly if the loading decreased. (The drawback to low density is the need for larger volumes of waste material to stabilize a large inventory of cesium and strontium.) However, as the material sinters, the grain coalesce, the pores consolidate, and the resulting material has a modest thermal conductivity (Fig. 5). The effective thermal conductivity k_{ef} of 1.50–1.95 W/m/K from ambient to 1000 °C is within the range calculated by Murashov for zeolites [23], and the range reported for highly porous mullite, $Al_6Si_2O_{13}$ samples [24]. This value is consistent with a model of a solid, continuous phase containing disconnected pores. Using the model described in [24] for a continuous solid phase containing a network of isolated pores,

$$k_{ef} = k_o\left[\frac{1+2\chi-2V(\chi-1)}{1+2\chi+V(\chi-1)}\right] \quad (1)$$

Table 3
Increase in concentration of some elements after sintering shows no loss of volatile cesium ('overall' groups the data from 600–1000 °C and compares to the initial loading of sample).

	Initial	600 °C	800 °C	1000 °C	Overall
Cs/Al	1.097 ± 0.014	1.129 ± 0.015	1.110 ± 0.012	1.081 ± 0.012	1.106 ± 0.008
Sr/Al	0.580 ± 0.009	0.561 ± 0.009	0.572 ± 0.008	0.562 ± 0.008	0.565 ± 0.005
Ba/Al	1.544 ± 0.021	1.477 ± 0.021	1.519 ± 0.020	1.469 ± 0.019	1.489 ± 0.011
Rb/Al	0.203 ± 0.004	0.206 ± 0.004	0.204 ± 0.004	0.201 ± 0.004	0.204 ± 0.002

where $\chi = \frac{k_o}{k_{inclusion}}$, and V is the volume fraction of the gaseous inclusions, we can estimate the thermal conductivity at theoretical density. Using $k_{inclusion}$ = 0.04 W/m/K for the air trapped in the pores, and V = 0.45, k_o = 3.3–4.4 W/m/K using data from Fig. 5 for k_{ef}.

5. Conclusions

We sintered to 1000 °C bentonite clay samples with up to 29% by mass of cesium, strontium, rubidium, and barium. The true density of the sintered product was 3 g/cm^3. There was an increase in porosity (~20%) with an increase in waste loading (~20%) for samples prepared with the chloride feed solution. We could not detect any loss of cesium during sintering. Instead, there was an increase in crystallinity of the waste form upon sintering to 1000 °C. The nitrate feed produced various cesium pollucite phases while the chloride feed did not produce these familiar phases. In fact, the X-ray diffraction peaks could not be matched to known cesium phases. Assemblages of silicates were formed that incorporated the Sr, Rb, and Ba ions. Gas evolution during sintering to 1000 °C was significant with significant water being evolved at approximately 600 °C.

Acknowledgments

The electron microscopy was accomplished at the Electron Microscopy Center for Materials Research at Argonne National Laboratory, a US Department of Energy Office of Science Laboratory operated under Contract No. DE-AC02-06CH11357 by UChicago Argonne, LLC. This work was supported by the US Department of Energy Department of Nuclear Energy Science and Technology under the Global Nuclear Energy Partnership.

References

[1] D. Gombert, R. Counce, A. Cozzi, J.V. Crum, W. Ebert, C. Jantzen, J. Jerden, R. Jubin, M. Kaminski, V. Maio, J. Marra, T. Nenoff, R. Scheele, H. Smith, B. Spencer, D. Strachan, J. Vienna, Global Nuclear Energy Partnership Integrated Waste Management Strategy Waste Treatment Baseline Study Volume I, GNEP-WAST-AI-RT-2007-000324, September 2007.
[2] M.D. Kaminski, J. Nucl. Mater. 347 (1–2) (2005) 94.
[3] M.D. Kaminski, J. Nucl. Mater. 347 (1–2) (2005) 104.
[4] L.P. Hatch, Am. Scientist (1953) 410.
[5] D. Strachan, W. Shulz, Glass and Ceramic Materials for the Immobilization of Megacurie-Amounts of Pure Cesium-137, ARH-SA-246, April 1976.
[6] I. MacLaren, J. Cirre, C.B. Ponton, J. Am. Ceram. Soc. 82 (11) (1999) 3242.
[7] K. Yanagisawa, M. Nichioka, N. Yamasaki, J. Nucl. Sci. Technol. 24 (1) (1987) 51.
[8] I.V. Chernyshova, Y.V. Semenov, V.M. Agoshov, M. Gambino, P. Gaune, J.P. Bros, Thermochim. Acta 175 (1991) 119.
[9] H. Mimura, K. Akiba, M. Ozawa, Preparation of ceramic solid forms immobilizing cesium and/or strontium and evaluation of their physical and chemical properties, in: International Conference Nuclear Energy for New Europe 2002, Kranjska Gora, Slovenia, 9–12 September 2002.
[10] C.A. Sorrell, The American Mineralogist, vol. 47, March–April 1962.
[11] J. Tripp, T. Garn, R. Boardman, J. Law, Sep. Sci. Technol. 41 (10) (2006) 2147.
[12] N.G. Vasil'eva, N.N. Anshits, O.M. Sharonova, M.V. Burdin, A.G. Anshits, Glass Phys. Chem. 31 (5) (2005) 637.
[13] C.L. Riddle, J.D. Baker, J.D. Law, C.A. McGrath, D.H. Meikrantz, B.J. Mincher, D.R. Peterman, T.A. Todd, Solvent Extr. Ion Exch. 23 (3) (2005) 449.
[14] J.D. Law, R.S. Herbst, D.R. Peterman, R.D. Tillotson, T.A. Todd, Nucl. Technol. 147 (2) (2004) 284.
[15] <http://www.ne.doe.gov/AFCI/neAFCI.html>.
[16] R.A. Wigeland, T.H. Bauer, T.H. Fanning, E.E. Morris, Nucl. Technol. 154 (2006) 95.
[17] Y.S. Sayi, C.S. Yadav, P.S. Shankaran, G.C. Chhapru, K.L. Ramakumar, V. Venugopal, Int. J. Mass Spectrom. 214 (2002) 375.
[18] E. Hoinkas, H. Matiske, J. Nucl. Mater. 223 (1995) 218.
[19] C.W. Parmalee, V.D. Frechette, J. Am. Chem. Soc. 25 (4) (1942) 108.
[20] M. Lambregts, S. Frank, Microporous Mesoporous Mater. 64 (2003) 1.
[21] G. Cerefice, L. Ma, M. Kaminski, Microscopic and Spectroscopic Characterization of Aluminosilicate Waste form with Cs/Sr Loaded Using SEM, TEM and XRD, Presented at The Minerals, Metals & Materials Society 2009 Annual Meeting and Exhibition, San Francisco, California, 15–19 February 2009.
[22] J.A. Fortner, S.B. Aase, D.T. Reed, in: B. Peter McGrail, Gustavo A. Cragnolino (Eds.), Scientific Basis for Nuclear Waste Management XXV MRS Proceedings, vol. 713, 2002, p. JJ11.37.
[23] V. Murashov, J. Phys.: Condens. Matter 11 (1999) 1261.
[24] R. Barea, M.I. Osendi, J.M.F. Ferreira, P. Miranzo, Acta Mater. 53 (11) (2005) 3313.